

Spectral Dynamics of Nitro-Derivatives of Xanthione in Solutions

Stanislav L. Bondarev, Sergei A. Tikhomirov, Oleg V. Bugarov, Valery N. Knyukshto, Nikolaii A. Galinovskii, Roman G. Fedunov, Svetlana S. Khohlova, and Anatoly I. Ivanov

J. Phys. Chem. A, **Just Accepted Manuscript** • DOI: 10.1021/acs.jpca.8b11146 • Publication Date (Web): 07 Feb 2019

Downloaded from <http://pubs.acs.org> on February 12, 2019

Just Accepted

"Just Accepted" manuscripts have been peer-reviewed and accepted for publication. They are posted online prior to technical editing, formatting for publication and author proofing. The American Chemical Society provides "Just Accepted" as a service to the research community to expedite the dissemination of scientific material as soon as possible after acceptance. "Just Accepted" manuscripts appear in full in PDF format accompanied by an HTML abstract. "Just Accepted" manuscripts have been fully peer reviewed, but should not be considered the official version of record. They are citable by the Digital Object Identifier (DOI®). "Just Accepted" is an optional service offered to authors. Therefore, the "Just Accepted" Web site may not include all articles that will be published in the journal. After a manuscript is technically edited and formatted, it will be removed from the "Just Accepted" Web site and published as an ASAP article. Note that technical editing may introduce minor changes to the manuscript text and/or graphics which could affect content, and all legal disclaimers and ethical guidelines that apply to the journal pertain. ACS cannot be held responsible for errors or consequences arising from the use of information contained in these "Just Accepted" manuscripts.



Spectral Dynamics of Nitro-Derivatives of Xanthione in Solutions

Stanislav L. Bondarev,[†] Sergei A. Tikhomirov,[†] Oleg V. Buganov,[†] Valeri N.
Knyukshto,[†] Nikolaii A. Galinovskii,[‡] Roman G. Fedunov,[¶]
Svetlana S. Khokhlova,[¶] and Anatoly I. Ivanov*,[¶]

[†]*B. I. Stepanov Institute of Physics, National Academy of Sciences of Belarus, Prospect
Nezavisimosti 68, Minsk BY-220072, Republic of Belarus*

[‡]*Institute of Chemistry of New Materials, National Academy of Sciences of Belarus, 36,
Fr. Skaryna Street, Minsk BY-220141, Republic of Belarus*

[¶]*Volgograd State University, University Avenue 100, Volgograd 400062, Russia*

E-mail: Anatoly.Ivanov@volsu.ru

Abstract

Nitro-derivatives of xanthione, 2,7-dinitro-9H-xanthene-9-thione and 2,4,7-trinitro-9H-xanthene-9-thione, have been first synthesized and their stationary and transient spectra have been measured. The stationary spectra show that the attachment of the nitro-groups to the xanthione scaffold leads to strong quenching of $S_2 \rightarrow S_0$ fluorescence and the decrease of the oscillator strength of the $S_2 \leftarrow S_0$ electronic transition. Analysis of the transient absorption spectra uncovers the ultrafast stimulated emission quenching from the second excited state, S_2 , in the both derivatives. A kinetic scheme has been suggested to rationalized the complex spectral dynamics of transient absorption signal. The kinetic scheme is deduced from the analysis of the transient spectra and supported by the quantum-chemical calculations which predict existence of a dark state and S_2 state splitting into two close levels. The ultrafast transitions between S_2 state sublevels and transition into the dark state play crucial role in spectral dynamics. These new features discovered in the nitro-derivatives of xanthione distinguish essentially their spectral dynamics from that observed in xanthione.

Introduction

Considerable interest of researchers in thioketones during past decades is associated with their remarkable spectral and photophysical properties.¹⁻⁶ Spectral properties are closely related to the electronic structure of their highest excited electronic states.³ For the thioketones in solutions experimentalists can distinguish separate S_1 , S_2 , and S_3 absorption bands, as well as direct absorption $T_1 \leftarrow S_0$, thermally activated delayed fluorescence from S_1 state, fluorescence and phosphorescence from S_2 and T_2 , correspondingly.⁷ The essential feature of thioketones is strong fluorescence from the second excited state and negligible one from the first excited state that is a bright example of the Kasha's rule violation.^{2,5,8,9} The latter is caused by the large energy gap between S_2 and S_1 states¹⁰ and appears in S_2 long lifetimes of thioketones $\tau \sim 10^{-9} - 10^{-11}$ s.^{1,4,7}

1
2
3
4
5
6
7
8
9
10
11
12
13
14
15
16
17
18
19
20
The second peculiarity of thioketones is the dependence of the phosphorescence quantum yield on the excitation wavelength. The triplets quantum yield, ϕ_T , for xanthione (XT) was shown to be close to unity upon the excitation into the first excited state, S_1 , while it is smaller than unity ($\phi_T = 0.5 - 0.6$) in the case of excitation into S_2 state.¹¹ It is a manifestation of the breakdown of the classical Vavilov-Kasha's law^{9,12} stating that the quantum yield of luminescence is independent of excitation wavelength. Besides, Vavilov-Kasha's law violation was observed for XT derivative, 4H-1-benzopyran-4-thione,¹³ for which the $S_2 \rightarrow S_0$ fluorescence yield, ϕ_f , under excitation into the absorption band $S_4 \leftarrow S_0$ decreases by 25% comparing with that at the excitation of $S_2 \leftarrow S_0$ band.

21
22
23
24
25
26
27
28
29
30
31
32
33
34
35
36
37
38
39
40
41
42
43
44
Input of large excess of vibrational energy in highly excited singlet states is often accompanied by photochemical processes of electron and proton transfer or isomerization, which do not always result in the irreversible formation of products. In the case of ineffective transitions to the triplet states, the electron excitation energy non-radiatively deactivates into the environment. Such non-radiative processes are named "induced internal conversion" $S_n \rightarrow S_0$ ($n = 1, 2, 3, \dots$),^{14,15} and also known as transition to the "dark state".¹⁶ For example, the quantum yield of $S_2 \rightarrow S_0$ fluorescence in XT is very small ($\phi_f \sim 0.05$)⁷ and the decrease of the quantum yield ϕ_T upon excitation in the S_2 state comparing to excitation into S_1 state is explained by the appearance of an effective $S_2 \rightarrow S_0$ internal conversion,^{3,11} while in DNA nucleobases (adenine, thiamine, guanine, etc.) practically the entire electron excitation energy deactivates through the internal conversion $S_1 \rightarrow S_0$ with rate constant $k_{ic} \sim 10^{12} \text{ s}^{-1}$.¹⁴

45
46
47
48
49
50
51
52
53
54
55
56
57
58
59
60
Experimental and theoretical studies of the dynamics of highly excited singlet states of xanthone^{16,17} and its derivatives^{18,19} have shown that upon the excitation of xanthone molecule to the singlet S_2 (π, π^*)-state the direct or indirect intersystem crossings to the lower T_1 -state occur with a very large probability due to high rate $k_{ISC} \sim 10^{11} \text{ s}^{-1}$. Such a high efficiency of intersystem crossings in xanthone is caused by close arrangement of singlet S_1 (n, π^*), S_2 (π, π^*) and triplet T_1 (n, π^*), T_2 (π, π^*) states, which can change their mutual

1
2
3 arrangement depending on the polarity of the solvent.^{16,17} In particular a strong dependence
4 of the fluorescence yield on the polarity of the solvent is observed for thioxanthone.¹⁸ Thus,
5 in cyclohexane fluorescence yield, ϕ_{fl} , equals 0.0002, and in 2,2,2-trifluoroethanol the yield is
6 0.46, and the fluorescence spectrum exhibits noticeable solvatochromism.¹⁸ At present there
7 are two conceptions of the energy deactivation mechanism of the S_2 state in thioxanthone.
8 The first one presents the mechanism of S_2 deactivation as the process $S_2(\pi, \pi^*) \rightarrow T_1(\pi, \pi^*)$
9 which lasts 4.0 ps. The second conception supposes that the S_2 quenching is the two-
10 stage process with lifetime constants $\tau_1 = 0.4$ ps [$S_2(\pi, \pi^*) \rightarrow S_1(n, \pi^*)$] and $\tau_2 = 4.0$ ps
11 [$S_1(n, \pi^*) \rightarrow T_1(\pi, \pi^*)$].¹⁸

12
13 A strong effect on the probabilities of non-radiative processes in another xanthone deriva-
14 tive, 2,7-diaminoxanthone,¹⁹ is rendered by the nature of the substituent (the electron-
15 donating properties of amino-group) as well as the proton-donating properties of solvents,
16 such as alcohols, which may form complexes with hydrogen bonds interacting with the amino-
17 groups of the 2,7-diaminoxanthone molecule, followed by quenching of its fluorescence.

18
19 The relatively long-lived second excited state in thioketones (S_2 and T_1) makes these
20 systems promising as elements of molecular electronic devices and, in particular, as light
21 switches. The existence of two or more long-lived states which can be selectively populated
22 with a photoexcitation pulse is necessary for the operation of such light switches. A pos-
23 sibility to design optical switches operating in the frequency range up to tens of GHz and
24 providing a high yield (up to 90%) of the charge separation process requires experimental-
25 ists and theorists to consider derivatives of thioketones with strong electron donor groups.²⁰
26 Besides, it requires detailed studies of the mechanisms of pico- and femtosecond deactivation
27 processes of highly excited singlet and triplet states of heterocyclic compounds.^{6,20-22}

28
29 A number of preliminary results obtained for XT and its derivatives^{6,19,21} allows outlining
30 the subsequent course of experimental and theoretical studies to construct a molecular model
31 with the desired frequency and charge parameters. In particular, for 1,3-dimethoxy-9H-
32 xanthene-9-thione (DXT)⁶ significant charge transfer (about 0.1 of the electron charge) was
33
34
35
36
37
38
39
40
41
42
43
44
45
46
47
48
49
50
51
52
53
54
55
56
57
58
59
60

1
2
3 observed from the methoxy group to the thiocarbonyl group, and the fitting of transient
4 absorption spectra of XT and DXT showed an increase in the intersystem crossing probability
5 of $S_1 \rightarrow T_1$ upon attaching electron-donor methoxy groups to the xanthione molecule.
6
7

8
9 Considering the results of the studies,^{6,19} we synthesized two nitro-derivatives of XT
10 with pronounced electron-acceptor properties: 2,7-dinitro-9H-xanthene-9-thione (DNXT)
11 and 2,4,7-trinitro-9H-xanthene-9-thione (TNXT). We provided complex experimental (sta-
12 tionary luminescent and transient absorption femtosecond measurements) and theoretical
13 (non-stationary density functional theory) studies of their photodynamics and the spectral-
14 kinetic characteristics of the new charge-transfer states arising for them. The main attention
15 was paid to clarifying all the channels of non-radiative deactivation of the electron excitation
16 energy in the XT molecule and its nitro-derivatives, on the basis of which the energy scheme
17 of the electronic transitions of the proposed optical switch can be constructed. In the article
18 we discuss in detail only the DNXT properties while a major part of information on TNXT
19 is presented in the Supporting Information.
20
21
22
23
24
25
26
27
28
29
30

31 The aims of this work are: (i) synthesis of DNXT and TNXT, (ii) study of its spectral
32 properties including the spectral dynamics, (iii) identification of the kinetic scheme of elec-
33 tronic transitions to fit the theoretical spectral dynamics to that measured for DNXT, (iv)
34 estimation of the rate constants of electronic transitions which are triggered by an excitation
35 of the fluorophore to the second excited state.
36
37
38
39
40
41
42

43 Experimental and Theoretical Methods

44
45
46 Xanthione and its nitro-derivatives, DNXT and TNXT, have been transformed from cor-
47 responding ketones by Lawesson's reagent using methods described in ref 23. Obtained
48 thioxanthenes have been purified using standard techniques: HPLC and thin-layer chro-
49 matography. Their purity have been measured by IR, ^1H , ^{13}C NMR spectroscopy and gas
50 chromatography. The detailed description of DNXT and TNXT synthesis and their purity
51
52
53
54
55
56
57
58
59
60

checking are provided below.

Xanthone (1.57 g, 8.00 mmol) and Lawesson's reagent (1.63 g, 4.04 mmol) have been dissolved in dry benzene (15 mL) and boiled for 2 h with stirring. The reaction has been monitored by thin layer chromatography (eluent petroleum ether/diethylether 19:1). The pre-dried silica gel (10 g) has been added to the reaction mixture. The benzene has been evaporated under reduced pressure. The dry residue has been chromatographed (eluent petroleum ether/diethyl ether 98:2). Finally 9H-xanthene-9-thione has been obtained with the yield 1.25 g (74%). M.p. 155 °C (lit. 157–178 °C). ^1H NMR (DMSO- d_6 , 500 MHz), δ : 7.48–7.51 (2H, m, H⁵, H⁷), 7.69 (2H, d, J 6.8 Hz, H¹, H⁸), 7.92–7.95 (2H, m, H⁴, H⁵), 8.59 (2H, d, J 6.8 Hz, H³, H⁶). ^{13}C NMR (DMSO- d_6 , 125 MHz) δ : 116.2, 125.9, 128.7, 129.6, 136.6, 150.6, 204.5 (C=S). EIMS (m/z): 212.03 (M+).

2,7-Dinitro-9H-xanthen-9-one (0.1 g, 0.3 mmol) and Lawesson's reagent (0.1 g, 0.3 mmol) have been dissolved in dry toluene (1 mL) and boiled for 2 h with stirring. The reaction has been monitored by thin layer chromatography (eluent petroleum ether/diethylether 19:1). The pre-dried silica gel (1 g) has been added to the reaction mixture. The toluene was evaporated under reduced pressure. The dry residue has been chromatographed (eluent petroleum ether/diethyl ether 98:2). Finally 2,7-dinitro-9H-xanthene-9-thione has been obtained with yield 0.074 g (82%). M.p. 193–197 °C. IR (KBr, ν cm^{-1}): stretch symmetric and asymmetric frequencies of NO₂ groups are at 1344 and 1540, stretch frequencies of C=S group at 1252–1182. ^1H NMR (CDCl₃, 500 MHz), δ : 7.68 (2H, d, J 9 Hz, H⁴, H⁵), 8.51 (2H, dd, J₁ 9 Hz, J₂ 3 Hz, H³, H⁶), 9.47 (2H, d, J 3 Hz, H¹; H⁸). ^{13}C NMR (CDCl₃, 125 MHz) δ : 120.0, 123.0, 127.0, 129.9, 140.4, 156.6, 204.8 (C=S). EIMS (m/z): 302.00 (M+).

2,4,7-trinitro-9H-xanthen-9-one (0.1 g, 0.3 mmol) and Lawesson's reagent (0.1 g, 0.3 mmol) have been dissolved in dry toluene (1 mL) and boiled for 2 h with stirring. The reaction has been monitored by thin layer chromatography (eluent petroleum ether/diethylether 19:1). The pre-dried silica gel (1 g) has been added to the reaction mixture. The toluene was evaporated under reduced pressure. The dry residue has been chromatographed (eluent

1
2
3 petroleum ether/diethyl ether 98:2). Finally 2,4,7-trinitro-9H-xanthene-9-thione has been
4 obtained with yield 0.1 g (96%). M.p. 201–202 °C. IR (KBr, ν cm⁻¹): stretch symmetric
5 and asymmetric frequencies of NO₂ groups are at 1340 and 1542, stretch frequencies of C=S
6 group at 1252–1184. ¹H NMR (CDCl₃, 500 MHz), δ : 7.79 (1H, d, J 9 Hz, H⁵), 8.67 (1H,
7 dd, J1 9 Hz, J2 3 Hz, H⁶), 9.17 (1H, d, J 3 Hz, H⁸), 9.40 (1H, d, J 3 Hz, H¹), 9.64 (1H, d,
8 J 3 Hz, H³); ¹³C NMR (CDCl₃, 125 MHz) δ : 120.0, 123.4, 127.0, 129.1, 129.9, 130.8, 136.9,
9 140.4, 141.3, 150.3, 156.6, 204.8 (C=S). EIMS (m/z): 346.98 (M+).

10
11 Cary-500 spectrophotometer (USA) has been utilized to register absorption spectra of
12 XT and DNXT in various solvents. The solvents (n-hexane, acetonitrile) were produced
13 by Merck (Sigma-Aldrich). Determination of the molar extinction coefficients has been
14 conducted by weighting of three samples of thioketone which have been dissolved later in a
15 certain volume of acetonitrile. The oscillator strengths have been estimated in accordance
16 with ref 19. A large-aperture setup has been used to detect the luminescence spectra in
17 a wide spectral range from 200 nm to 1000 nm. The details of a stationary and pump-
18 probe measurement setups have been described elsewhere.^{6,19,24–26} A pump signal has been
19 generated by the second harmonic of Al₂O₃:Ti³⁺ laser (395 nm) with the energy in a range
20 10 ~ 30 μ J. Sample has been prepared in 2 mm thick cell with dye concentration in a range
21 of 10⁻³ and 10⁻⁵ M. At the dye concentrations of 10⁻³ and 10⁻⁵ M the absorption and
22 fluorescence spectra are close to each other. The probe pulse being transmitted through the
23 water achieves white continuum ranging in 400 – 1100 nm from the fundamental laser beam
24 with $\lambda = 790$ nm. A polychromator with Hamamatsu S7031 – 1007S back-thinned type
25 CCD area image sensor had recorded the signal of probe and reference pulses which then
26 has been processed with special software on PC. The sensor has improved sensitivity in UV
27 region and high signal/noise ratio. The time-dependent signal of absorbance $\Delta D(\lambda, \Delta t)$ is
28 determined as $\Delta D(\lambda, \Delta t) = \lg(\tilde{T}_0/\tilde{T})$ where $\tilde{T} = E_{\text{prob}}/E_{\text{ref}}$ and $\tilde{T}_0 = E_{\text{prob}}^0/E_{\text{ref}}^0$ are the
29 energy ratios of the probe and reference pulses passed through the sample with and without
30 preceding pump, respectively. The correction of transient spectra accounts for the group
31
32
33
34
35
36
37
38
39
40
41
42
43
44
45
46
47
48
49
50
51
52
53
54
55
56
57
58
59
60

1
2
3 velocity dispersion of the probe pulse.
4

5 The GAMESS-US^{27,28} software package has been used for quantum chemical simulations.
6
7 The optimized structures of DNXT and TNXT have been calculated in the approximation
8 of an isolated molecule in the gas phase at DFT level. The density functional B3LYP (key-
9 word DFTTYP=B3LYP in \$CONTROL) in the 6-31G⁺⁺ basis set (keywords GBASIS=N31
10 NGAUSS=6 NDFUNC=1 DIFSPP=.TRUE. in \$BASIS) has been used. The initial guess for
11 wavefunction and type of calculation has been chosen to be RHF (keyword SCFTYPE=RHF
12 in \$CONTROL). The initial geometry has been C1 (without symmetry restrictions). The
13 geometry optimization in the ground and excited states has been carried out by the gradi-
14 ent method. The convergence criteria to end the optimization process has been set to 10^{-4}
15 (keyword OPTTOL=0.0001 in \$STARTPT). The solvent effect on the structure and spectra
16 has been accounted for within polarized continuum model (PCM). The effect of following
17 solvents have been studied: n-hexane (the static dielectric permittivity $d = 1.890$, the re-
18 fractive index $n^2 = 1.375$, and the solvent radius, $R_{\text{solv}} = 1.5$, keywords SOLVENT=input
19 EPS=1.890 EPSINF=1.375 RSOLV=1.5 in \$PCM) and acetonitrile ($d = 36.6$, $n^2 = 1.807$,
20 $R_{\text{solv}} = 1.5$, keywords SOLVENT=input EPS=36.6 EPSINF=1.807 RSOLV=1.5 in \$PCM).
21 The time-dependent density functional theory (TDDFT) has been applied to calculate the en-
22 ergies of electronic transitions (keywords TDDFT=excite in \$CONTROL and NSTATE=30
23 IROOT= i SG1=.TRUE. in \$TDDFT, where i denotes corresponding excited state). Because
24 of a very slow convergence of the geometry optimization cycles for excited state in solvents,
25 the calculations have been stopped at the tolerance parameter $5 \cdot 10^{-4}$ (n-hexane) and 10^{-3}
26 (acetonitrile).
27
28
29
30
31
32
33
34
35
36
37
38
39
40
41
42
43
44
45
46
47
48

49 Results and Discussion

50
51
52 The calculation results of energetic and electronic properties of 2,7-dinitro-9H-xanthene-9-
53 thione (DNXT) are listed in Tables 1 and 2. It should be noted that the solvent influence
54
55
56
57
58

on the solute are calculated within the electrostatic interaction approximation (PCM). The energies of the solute-solvent interaction in the excited states are estimated by using the equilibrium electronic structure of the ground electronic state. The geometry and electronic structure of DNXT in the ground state is presented in Figure 1, the information on TNXT is presented in Supporting Information. The bond lengths, bond angles, and atomic charges, indicated in the Figure 1, are calculated using the DFT/B3LYP method for the equilibrium geometry of the ground state in the gas phase. The lengths of characteristic bonds in the ground state of DNXT in two solvents, listed in the Table 1, were optimized using the same method, and the TDDFT/B3LYP method for excited states. The DNXT geometry structure in the ground state obtained in n-hexane and acetonitrile matches its gas phase geometry. In the first excited electronic state, the DNXT geometry slightly differs from that listed in Figure 1 for the pyran and benzene rings. Alterations in the bond lengths and bond angles are $\pm 0.01 \text{ \AA}$ and $\pm 2^\circ$, respectively. The bond length R_{S1-C2} has only a valuable deformation upon the excitation.

Table 1: The energetic characteristics of DNXT in the ground and excited electronic states obtained in the equilibrium geometry. S_i , Max.grad. (in Hartree/Bohr), E_{toti} , E_{EI} , E_{HOMO} , E_{LUMO} (in eV), μ (in Db), R_{S1-C2} , R_{C2-C3} , R_{C3-C4} , R_{C4-C5} , $R_{C14-N16}$ (in \AA) are the i -th electronic state, the maximum gradient achieved during optimization, the total energy, the energy of the electrostatic interaction of a solute with solvent, the energy of the highest occupied molecular orbital, the energy of the lowest unoccupied molecular orbital, the dipole moment, and the bond lengths, respectively.

No	S_i	Max.grad.	Solvent	E_{toti}	E_{EI}	E_{HOMO}	E_{LUMO}	μ	R_{S1-C2}	R_{C2-C3}	R_{C3-C4}	R_{C4-O7}	$R_{C14-N16}$
1	S_0	$1.0 \cdot 10^{-4}$	vacuum	-37608.35	-	-6.76	-3.66	6.64	1.66	1.47	1.41	1.36	1.47
2	S_0	$1.0 \cdot 10^{-4}$	n-hexane	-37608.33	-0.24	-6.68	-3.55	7.87	1.66	1.47	1.41	1.36	1.47
3	S_1	$1.0 \cdot 10^{-4}$	n-hexane	-37606.68	-0.25	-6.51	-3.73	5.07	1.74	1.43	1.42	1.36	1.47
4	DS_1	$1.0 \cdot 10^{-4}$	n-hexane	-37606.06	-0.26	-6.50	-3.73	9.82	1.70	1.44	1.42	1.33	1.45
5	S_2	$5.5 \cdot 10^{-4}$	n-hexane	-37605.32	-0.26	-6.49	-3.73	8.86	1.74	1.43	1.43	1.34	1.46
6	S_3	$8.9 \cdot 10^{-3}$	n-hexane	-37605.23	-0.26	-6.47	-3.74	8.86	1.75	1.43	1.43	1.35	1.45
7	S_0	$1.0 \cdot 10^{-4}$	acetonitrile	-37608.20	-0.66	-6.60	-3.45	9.97	1.66	1.47	1.41	1.36	1.47
8	S_1	$1.0 \cdot 10^{-4}$	acetonitrile	-37606.19	-0.72	-6.47	-3.62	6.86	1.74	1.43	1.42	1.36	1.46
9	DS_1	$1.0 \cdot 10^{-4}$	acetonitrile	-37605.61	-0.75	-6.49	-3.63	6.07	1.70	1.44	1.42	1.35	1.43
10	S_2	$2.7 \cdot 10^{-4}$	acetonitrile	-37605.65	-0.74	-6.49	-3.66	11.02	1.70	1.44	1.42	1.34	1.43
11	DS_2	$1.0 \cdot 10^{-4}$	acetonitrile	-37605.27	-0.72	-6.49	-3.60	5.72	1.70	1.44	1.42	1.36	1.44

Here we use S_1 , S_2 , and S_3 to denote the local excited states while the excited state with zero or close to zero oscillator strength (Ds) are called "dark states". The dark states

Table 2: The charges (in the units of the elementary charge) located on the atoms of DNXT molecule. The numbers in the first column correspond to the numbering given in the first column of Table 1.

No	S1	C2	C3	C4	C5	C6	O7	C8	C11	C12	C15	N17	O18	O19	H23
1	-0.26	0.12	1.83	-0.65	1.80	-0.59	-0.39	-0.57	0.12	-0.33	-0.51	-0.34	0.00	-0.01	0.27
2	-0.26	0.12	1.83	-0.65	1.80	-0.59	-0.39	-0.57	0.12	-0.33	-0.51	-0.34	0.00	-0.01	0.27
3	0.06	-0.22	0.21	0.33	0.21	0.33	-0.45	-0.23	-0.23	-0.38	0.13	0.32	-0.32	-0.26	0.25
4	0.23	-0.15	0.18	0.35	0.19	0.29	-0.41	-0.23	-0.23	-0.36	0.15	0.24	-0.45	-0.38	0.25
5	-0.32	0.22	1.77	-0.62	1.78	-0.51	-0.36	-0.56	0.20	-0.36	-0.63	-0.37	-0.01	-0.02	0.28
6	-0.31	0.25	1.78	-0.59	1.77	-0.53	-0.36	-0.58	0.18	-0.34	-0.64	-0.33	-0.02	-0.03	0.28
7	-0.35	0.15	1.96	-0.65	1.92	-0.59	-0.36	-0.58	0.18	-0.30	-0.70	-0.27	-0.07	-0.06	0.27
8	0.07	-0.23	0.22	0.33	0.22	0.33	-0.43	-0.23	-0.22	-0.38	0.14	0.34	-0.35	-0.30	0.25
9	0.28	-0.16	0.21	0.33	0.21	0.33	-0.40	-0.21	-0.22	-0.35	0.15	0.29	-0.38	-0.44	0.26
10	-0.38	0.24	1.88	-0.61	1.87	-0.53	-0.35	-0.58	0.26	-0.35	-0.73	-0.34	-0.06	-0.06	0.27
11	0.27	-0.16	0.21	0.33	0.21	0.33	-0.43	-0.22	-0.22	-0.34	0.15	0.29	-0.37	-0.43	0.26

appearance opens new channels of the electronic transitions such as internal conversion from higher excited states. To simplify further analysis, transitions to two dark states are modeled by a transition to one dark state. The analysis of the Mulliken charges on DNXT atoms (see Table 2) has shown that molecular bonds in polar solvent (acetonitrile) is more polarized in comparison with that calculated in the gas phase or apolar solvent (n-hexane). However, the dipole moment direction in the first excited state matches its direction in the ground state. Note that excitation of DNXT results in a considerable variation of the atomic charges on the thiocarbonyl group (q_{S1}, q_{C2}). In the dark state the electronic structure of DNXT and TNXT significantly differs from that in the locally excited state in both polar and apolar solvents, which is associated with considerable charge transfer between the sulfur and both nitrogen atoms. This conclusion is approved by the analysis of the "lambda diagnostic" procedure (see details in SI).²⁹ It should be noted that quantum chemical calculations do not predict any dark states in XT lying between S_2 and S_1 states.

The electronic absorption and luminescence spectra of XT in apolar and polar solvents: n-hexane and acetonitrile are shown in Figure 2 A and B, correspondingly.

The absorption spectra are characterized by three vibronic bands in the UV region (280–320 nm, 320–360 nm, and 360–410 nm), which according to the literature^{1–3} corresponds to electronic transitions $S_4 \leftarrow S_0$, $S_3 \leftarrow S_0$ and $S_2 \leftarrow S_0$. The transitions $S_4 \leftarrow S_0$ and $S_2 \leftarrow S_0$

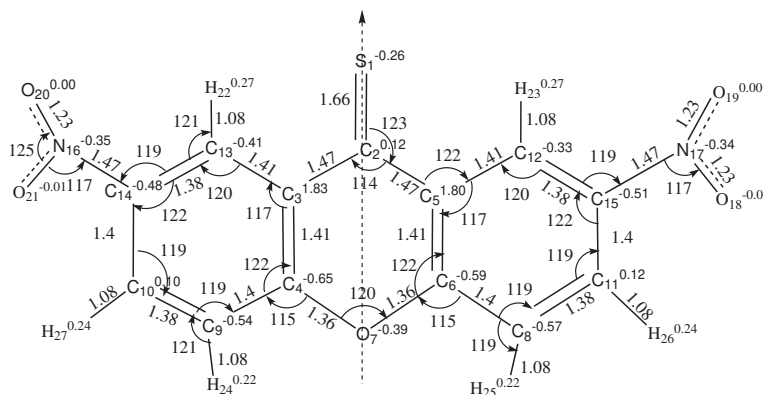


Figure 1: The equilibrium structure of the DNXT molecule in the ground electronic state calculated in the gas phase. All the parameters (charges, bond lengths, and angles) have been also calculated in the gas phase.

are allowed (π, π^*)-transitions and their molar extinction coefficients are $\varepsilon \geq 10^4 \text{ M}^{-1}\text{cm}^{-1}$. The low-intensity transition $S_0 \leftarrow S_3$ is forbidden in symmetry and it becomes allowed, for example, in 1,3-dimethoxy-9H-xanthene-9-thione, in which the symmetry is lower than that in the XT.⁶ The $S_0 \leftarrow S_1$ transition in the XT and its derivatives is strongly forbidden and its molar extinction coefficient is estimated to be $\varepsilon \simeq 20 \text{ M}^{-1}\text{cm}^{-1}$.²⁻⁵ Therefore, it practically appears neither in the absorption spectra nor in the fluorescence spectra (Figure 2 A). Such an unusual fact for the organic compounds spectroscopy is due to the presence of heteroatom of sulfur in the XT molecule. Its unshared pair of electrons participates in the $S_0 \leftarrow S_1$ electron transition and, accordingly, this transition is (n, π^*)-transition. For the same reason, phosphorescence is observed at room temperature, which spectrum in n-hexane is characterized by the resolved vibronic structure (Figure 2 A). The distances between the vibrational maxima in the fluorescence, $S_0 \leftarrow S_2$, and phosphorescence, $S_0 \leftarrow T_1$, spectra are approximately the same and amount $1200 \pm 40 \text{ cm}^{-1}$. This frequency corresponds to the frequency of the stretching vibration of the $\text{C} = \text{S}$ bond,³⁰ which indicates the main role of the S atom in the formation of the vibrational structure of the electron spectra of the XT. There is no visible vibronic structure in the XT spectra in acetonitrile, and a wide band appears at $\lambda_{\text{max}} = 686 \text{ nm}$ instead of pronounced structure with four maxima as it is in n-hexane (see insert in Figure 2 B).

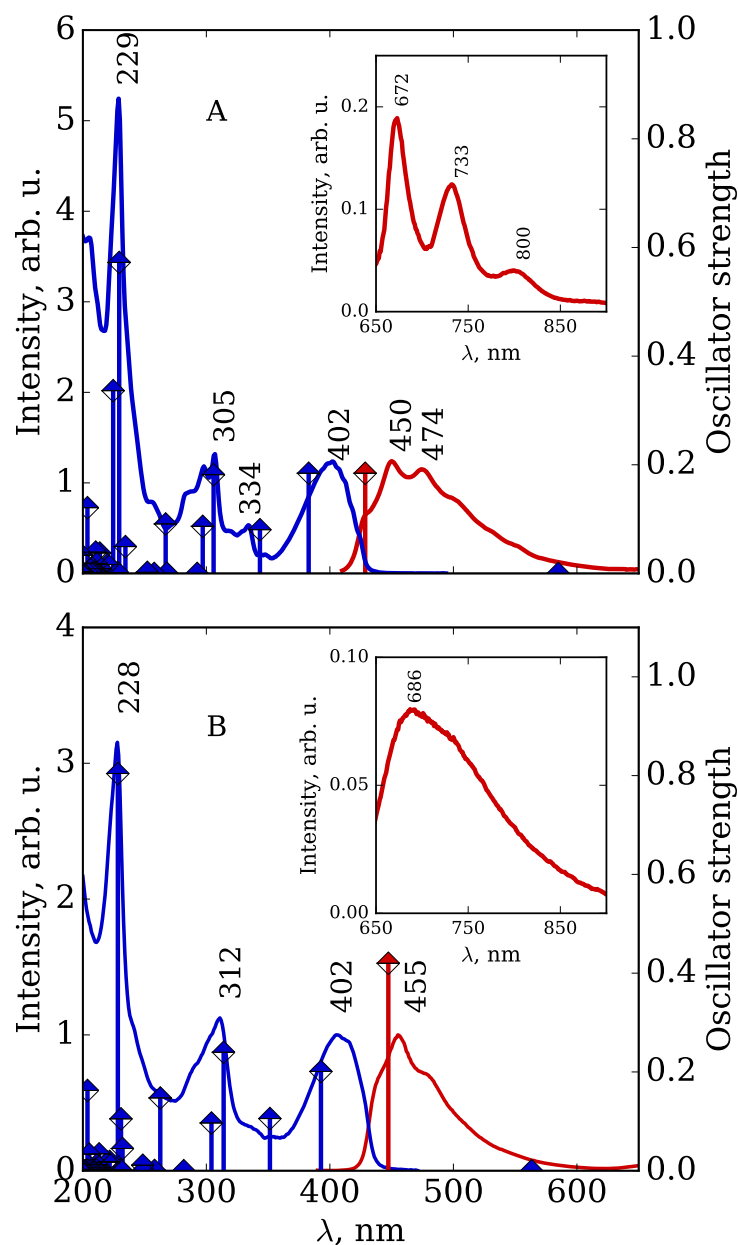


Figure 2: The absorption (blue) and luminescence (red) spectra of XT molecule in n-hexane (frame A) and acetonitrile (frame B) measured experimentally (solid lines) at 293 K and calculated theoretically (histogram). Inserts in the figure show phosphorescence spectra of XT in the region 650 – 900 nm.

Table 3: The spectral characteristics of XT, DNXT and TNXT in n-hexane. Here $\lambda_{\text{abs}}^{\text{max}}$ and $\lambda_{\text{fl}}^{\text{max}}$ are the wavelengths of the absorption and fluorescence band maxima, $\lambda_{\text{Ph}i}^{\text{max}}$ is the wavelength of the i -th vibronic phosphorescence band maximum, $E_{0,0}^{\text{fl}}$ and $E_{0,0}^{\text{Ph}}$ are the energy gaps for the $S_2 \leftarrow S_0$ and $T_1 \leftarrow S_0$ electronic transition between the 0-th vibronic sublevels, correspondingly, ΔE_{Ph} is the difference between the energy of the triplet levels in DNXT and XT, $\Delta E(S_2 - T_1)$ is the energy gap between the S_2 and T_1 electronic levels.

No	Molecule	$\lambda_{\text{abs}}^{\text{max}}$, nm	$\lambda_{\text{fl}}^{\text{max}}$, nm	$\lambda_{\text{Ph}1}^{\text{max}}$, nm	$\lambda_{\text{Ph}2}^{\text{max}}$, nm	$\lambda_{\text{Ph}3}^{\text{max}}$, nm	$E_{0,0}^{\text{fl}}$, cm^{-1}	$E_{0,0}^{\text{Ph}}$, cm^{-1}	ΔE_{Ph} , cm^{-1}	$\Delta E(S_2 - T_1)$, cm^{-1}
1	XT	402	450	673	733	798	22220	14860	-	7360
2	DNXT	394	444	711	777	854	22520	14060	800	8460
3	TNXT	390	426	732	806	885	23470	13660	1200	9810

Table 4: The spectral characteristics of XT, DNXT and TNXT in acetonitrile. Here f_{abs} and f_{fl} are the absorption and fluorescence band oscillator strengths, respectively, ε is the extinction coefficient, $E_{\text{fl}}^{\text{max}}$ and $E_{\text{Ph}}^{\text{max}}$ are the wavenumbers of the fluorescence and phosphorescence band maxima, respectively. The values of the absorption band oscillator strengths, f_{abs} , are measured while f_{fl} are calculated using the well known Einstein's relations. The definitions of the other observables are given in the caption of Table 3.

No	Molecule	$\lambda_{\text{abs}}^{\text{max}}$, nm	$\lambda_{\text{fl}}^{\text{max}}$, nm	ε , $\text{M}^{-1}\text{cm}^{-1}$	f_{abs}	f_{fl}	$\lambda_{\text{Ph}}^{\text{max}}$, nm	$E_{\text{fl}}^{\text{max}}$, cm^{-1}	$E_{\text{Ph}}^{\text{max}}$, cm^{-1}	ΔE_{Ph} , cm^{-1}	$\Delta E(S_2 - T_1)$, cm^{-1}
1	XT	406	455	17000	0.54	0.48	686	21980	14580	-	7400
2	DNXT	402	459	8500	0.31	0.27	745	21790	13420	1160	8370
3	TNXT	402	469	8700	0.32	0.27	800	21320	12500	2080	8820

When nitro-groups are attached to the XT scaffold, the phosphorescence spectra in both solvents are shifted to the long-wavelength region. However, fluorescence spectra demonstrate a hypsochromic shift in n-hexane and bathochromic shift in acetonitrile (see Tables 3 and 4). Such changes in the spectral-luminescent characteristics of the thioketones, depending on their structure and the polarity of the medium, testify that the energy gap $\Delta E(S_2 - T_1)$ increases as the redox potential of the thioketone molecule increases with the number of nitro-groups attached. Changes in the spectral properties due to attachment of a next nitro-group to the XT scaffold evidences on quenching of the luminescence that apparently is caused by the interaction of nitro-groups with the conjugated thioketone system (or in other words, caused by the charge transfer). The effect of charge transfer on the spectral properties of DNXT and TNXT also manifests itself in a significant decrease in their molar

1
2
3 extinction coefficients (about two times) and the oscillator strengths (1.7 times) as compared
4 to XT (See Table 4). This experimental fact apparently reflects the electron density trans-
5 fer from the conjugated system of the XT scaffold to electron-acceptor nitro-groups and a
6 corresponding decrease in its absorption capacity. The shift of the triplet level of the DNXT
7 and TNXT with respect to the XT, given in the column ΔE_{Ph} of Table 3 is of particular
8 interest. A large bathochromic shift of the T_1 level has been observed in acetonitrile for the
9 TNXT (see Supporting Information), which value amounts 2080 cm^{-1} . Quantum-chemical
10 calculation of the energy levels of the TNXT in the gas phase supports this observation (see
11 energy diagram S7 in the Supporting Information). Earlier we published data on the effect
12 of an electron-donor methoxy-group on the position of the T_1 -level in the XT molecule.⁶ In
13 n-hexane solution the T_1 -level of DXT is 850 cm^{-1} higher than the corresponding level in the
14 XT molecule. This result was interpreted in ref 6 as a convergence of the S_1 and T_1 levels in
15 the DXT molecule in comparison with the XT with a corresponding increase in the quantum
16 yield of the intersystem crossing. In the case of XT nitro-derivatives, the opposite effect
17 is observed, a decrease of the energy of the T_1 level, which amounts 2080 cm^{-1} for TNXT
18 in acetonitrile. In order to elucidate the mechanism of non-radiative deactivation of the
19 electron excitation energy in this case, we carried out experimental and theoretical studies
20 of the femtosecond spectral dynamics of the XT and its nitro-derivatives in acetonitrile.
21
22
23
24
25
26
27
28
29
30
31
32
33
34
35
36
37
38

39 The absorption and fluorescence spectra of DNXT in n-hexane and acetonitrile measured
40 experimentally (solid curves) and calculated theoretically (vertical lines) are demonstrated
41 in Figure 3. The number of observed experimental bands in the spectral window considered
42 are less than the number of excited states. The latter results in some problems in labeling
43 of the excited states. To maximize the correspondence we labeled the lowest singlet state as
44 S_1 which associates with the first weak but observable absorption band of XT and its nitro
45 derivatives: 570 nm (XT, $f = 0.0009$), 582 nm (DNXT, $f = 0.0012$), and 602 nm (TNXT,
46 $f = 0.0013$) in acetonitrile (not shown in Figure 3). Next two excited states having even
47 lesser oscillator strengths, hence, invisible in absorption spectrum are labeled as Ds_1 and
48
49
50
51
52
53
54
55
56
57
58
59
60

1
2
3 D_{S_2} . The second absorption band having much larger oscillator strength associates with two
4 excited states S_2 and S_3 .
5
6

7 In the absorption spectra calculated for both the solvents there are three well-defined
8 "doublets" (pairs of closely spaced lines of comparable intensity) which correspond to the
9 main experimental bands. In n-hexane they occupy the regions around 380 (S_2 and S_3 levels
10 in Table 1), 320, and 285 nm. The energy level scheme containing the singlet and triplet
11 states in the equilibrium geometry of the ground state in vacuum is demonstrated in Figure 4.
12 The transitions to the singlet excited states with nonzero oscillator strength are shown by
13 vertical arrows. The state with the energy about 2 eV is labelled as S_1 in Figure 4 while the
14 states located about 3.0 eV are called the "dark" states. In Figure 4 the oscillator strengths
15 shown in brackets and wavelengths of the transitions are listed above the arrows.
16
17
18
19
20
21
22
23
24

25 The transition energies calculated in the apolar (Figure 3 A) and polar (Figure 3 B)
26 solvents together with its oscillator strengths and those obtained experimentally for both the
27 absorption and fluorescence spectra of DNXT are in good agreement. As seen from Figure 3,
28 three main absorption bands have a doublet structure. Similar results were obtained earlier
29 for methoxy derivatives of XT that manifest itself in the broadening of the absorption band,
30 $S_2 \leftarrow S_0$.⁶
31
32
33
34
35
36

37 The experimental and simulated transient absorption spectra (TA) of DNXT are pre-
38 sented in Figure 5. The spectra of TNXT are shown in Supporting Information. The
39 measurements of DNXT and TNXT spectra in various solvents at room temperature were
40 carried out in the wavelength domain from $\lambda = 400$ to 740 nm for the time window from 1
41 ps to 100 ps (See Supporting Information). Since there is an overlap of the bleach band and
42 pump pulse at 395 nm, the part of the TA spectrum including part of bleach band is not
43 shown in figures. Nevertheless, TA signal kinetics at the red edge of the bleach are given in
44 Figures 7 and S9 (Supporting Information). The all measurements of DNXT has revealed an
45 excited state absorption band with the maximum near to $\lambda_{max} \simeq 635$ nm and gain spectra
46 in the region 420 – 520 nm. The positions of these bands are close to the band positions
47
48
49
50
51
52
53
54
55
56
57
58
59
60

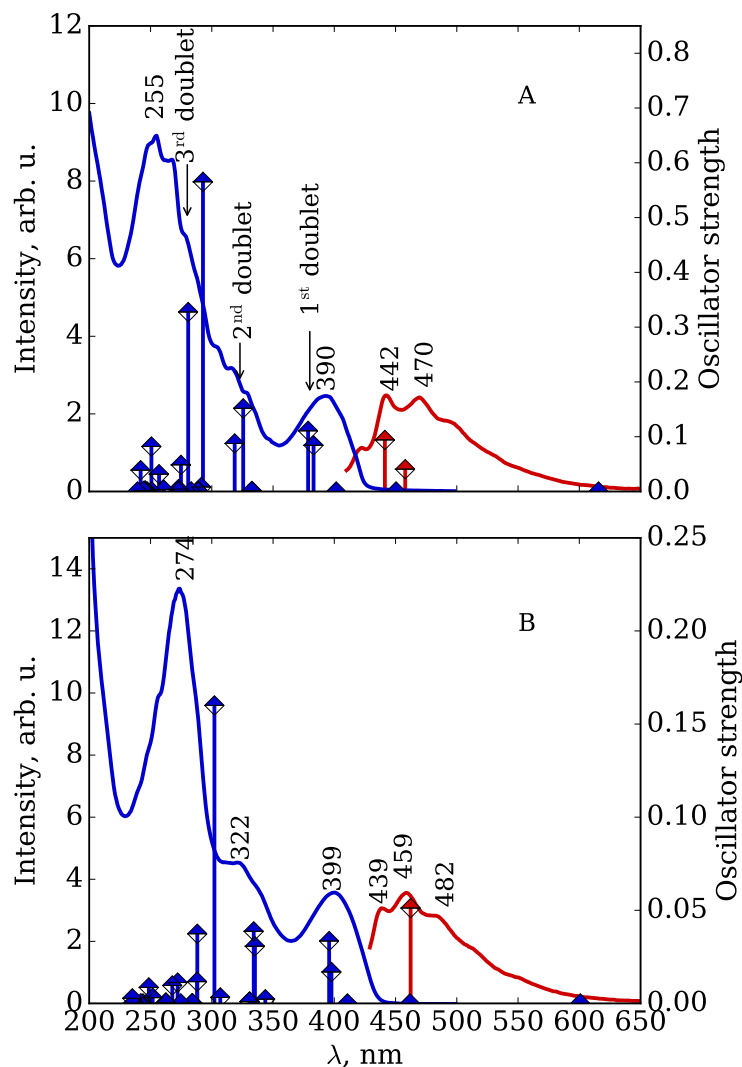


Figure 3: The absorption and luminescence spectra of DNXT in n-hexane (frame A) and acetonitrile (frame B). The solid lines correspond to experimental results for absorption (blue) and luminescence (red) measured at 293 K. The vertical lines show the oscillator strengths obtained from the quantum-chemical calculations. The red lines at the frame A corresponds to the transitions $S_2 \rightarrow S_0$ and $S_3 \rightarrow S_0$.

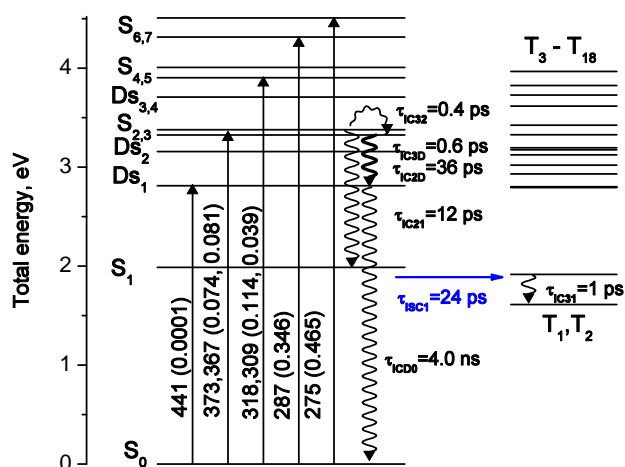


Figure 4: The diagram of energies of the stationary states and transitions between them obtained at DFT level for DNXT calculated in the gas phase. The arrows indicate the maxima of the transition bands with nonzero oscillator strengths (shown next to the arrows in parentheses). Their wavelengths are shown next to the arrows. The lifetime constants returned from the fitting to the spectral dynamics are also presented.

observed for the transient spectra of XT in the n-hexane (see Figure 2 in ref 6). However, there is an important difference between the transient spectra of DNXT measured in this work and of XT measured earlier. The stimulated emission is strongly suppressed in DNXT in the solvents of strong polarity (See Supporting Information). Apparently, the difference is due to the appearance of a new absorption band of the excited state overlapping with the stimulated emission band. The kinetics of the transient absorption signal of DNXT at 500 nm consist of two components which are similar to those in XT: the short component with a lifetime about 20 ps and long-lived one exceeding 100 ps. Apparently, the first short lifetime of 20 ps associates with the excited S_2 state decay and long time constant, probably, characterizes rising the triplet-triplet $T_k \leftarrow T_1$ absorption. Up to the moment of the first measuring with a delay of 0.4 ps a considerable part of S_3 state population deactivates resulting in suppression of the stimulated emission signal.

The simulated transient absorption spectra of DNXT in different solvents have been simulated on the approach elaborated in ref 31. This theory has already been approved for

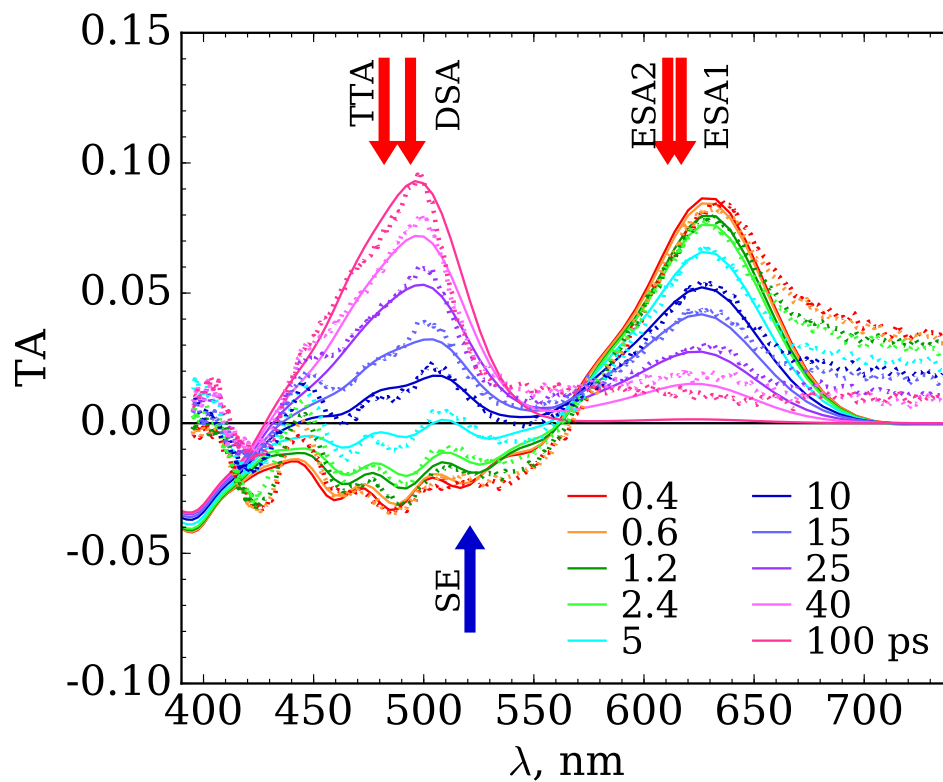


Figure 5: The experimental (dotted lines) and calculated (solid lines) transient absorption spectra of DNXT in acetonitrile at 293 K. The simulated spectra are obtained from the theoretical approach (7) – (11). All the energetic parameters are determined from the fitting and listed in Table 5. Arrows indicate the maxima of the corresponding bands after relaxation (see Table 5).

xanthione⁶ and xanthone¹⁹ derivatives as well as for pyrylium phenolate.³² The theory allows quantitatively and qualitatively reproducing of experimental transient absorption spectra.

Analysis of the experimental transient absorption spectra indicates that the total absorption signal

$$\Delta D(\nu_e, \nu_p, t) = \sum_i \Delta D_i(\nu_e, \nu_p, t) \quad (1)$$

in the case of DNXT molecule can be decomposed on bleach, ΔD_{BL} , stimulated emission, ΔD_{SE} , k excited state absorption bands, ΔD_{ESAK} , and triplet-triplet absorption, ΔD_{TTA} . Here ΔD_i are the values of the optical transition probabilities:

$$\Delta D_i(\nu_e, \nu_p, t) = \nu_p f_i \frac{V_{\text{pi}}^2}{P} \frac{\pi \tau_p}{\sigma_i(t)} \sum_{n,m} P_n \frac{e^{-\xi_i} \xi_i^m}{m!} \quad (2)$$

$$\times \exp \left[-\frac{(\delta \nu_{mi} - Q_{ni}(t))^2}{2\sigma_i^2(\tau)} \right] P(t) \quad (3)$$

where the index i may take one of the values: {ESAK, SE, BL, TTA}. $P(t)$ is the population of one electronic states: {S₃, S₂, S₁, Ds₁, T₁}, σ_i is the time-dependent half-width of the corresponding band:

$$\sigma_i^2(t) = \tau_p^{-2} + 2E_{ri}k_B T - (2E_{ri}k_B T X(t)/\sigma_e)^2 \quad (4)$$

and Q_{ni} is the coordinate of center-of-gravity of the corresponding band:

$$Q_{ni}(t) = 2E_{ri}X(t)(1 - \delta_{i,\text{BL}} + \delta \nu_{ne}k_B T/\sigma_e^2) \quad (5)$$

Here we used the following notions: $\sigma_e^2 = \tau_e^{-2} + 2E_{r\text{SE}}k_B T$, $\delta \nu_{ne} = \nu_e + \Delta G_{\text{SE}} - E_{r\text{SE}} - n\Omega_{\text{hf}}$, $\delta \nu_{m\text{ESAK}} = \nu_p + \Delta G_{\text{ESAK}} - E_{r\text{ESAK}} - m\Omega_{\text{hf}}$, $\delta \nu_{m\text{SE}} = \nu_p + \Delta G_{\text{SE}} + E_{r\text{SE}} + m\Omega_{\text{hf}}$, $\delta \nu_{m\text{BL}} = \nu_p + \Delta G_{\text{SE}} - E_{r\text{SE}} - m\Omega_{\text{hf}}$, $\delta \nu_{m\text{TTA}} = \nu_p + \Delta G_{\text{TTA}} - E_{r\text{TTA}} - m\Omega_{\text{hf}}$ are the solvent relaxation functions, where ΔG_i is the change of free energy for corresponding transition, E_{ri} and E_{rhi} are the reorganization energies of solvent and high-frequency mode for i -th

transition, respectively, excluding ESA band, Ω_{hf} is the frequency of the high-frequency mode for corresponding transition. $\delta_{i,\text{BL}}$ is the Kroneker's symbol. Here all the quantities Ω , ν , and $\delta\nu$ are measured in the energy units.

The probability of the transition generating n vibrational quanta at the pump stage can be represented in the following form:

$$P_n = \frac{\pi V_e^2 \tau_e}{\sigma_e} \frac{e^{-\xi_{\text{SE}}} \xi_{\text{SE}}^n}{n!} \exp \left[-\frac{(\delta\nu_{ne})^2}{2\sigma_e^2} \right] \quad (6)$$

where $P = \sum P_n$, $\xi_i = E_{\text{rhi}}/\Omega_{\text{hf}}$ is the Huang-Rhys factor, where τ_e , τ_p , ν_e , and ν_p are the durations and the carrier frequencies of the pump and probe pulses, V_e , and V_p are proportional to the matrix elements of the dipole moment of interaction with electromagnetic field. k_B and T are the Boltzmann constant and the temperature.

Since the intramolecular vibrational relaxation of high-frequency modes proceeds in the femtosecond timescale,³³ we assume that it is instant in comparison with the solvent vibrational relaxation. The solvent relaxation function is

$$X(t) = \sum_i x_i \exp \{-t/\tau_i\}, \quad \sum_i x_i = 1$$

where the solvent relaxation is modeled in the terms of a few Debye modes whose weights x_i and relaxation times τ_i was reported in ref 33.

At first, the simplest scheme of transitions elaborated earlier for the description of transient spectra in XT⁶ (see Figure 6 showing the experimental and simulated transient spectra of XT in acetonitrile), which does not involve the dark and S₃ states, was used. A comparison of the ratios of stimulated emission to ESA signals at a delay of 0.4 ps shows that the ratio in DNXT is about 6 times larger than that in XT. Since the experimental data show that the fluorescence oscillator strength in DNXT is 1.8 times smaller while the ESA signal is only 1.14 times larger than that in XT, so that it is impossible to fit the transient absorption spectra without an ultrafast S₂ state depopulation. This fact may indicate the important

1
2
3 role of the dark state (Ds_1) and the doublet structure of the second excited state (S_3 , S_2),
4 which is predicted by quantum-chemical calculations (see Figure 4). Given the similarity of
5 the structures of S_2 and S_1 states in XT and DNXT, one can expect that the rate constants
6 of the internal conversion $S_2 \rightarrow S_1$ are also close to each other. The quantum-chemical
7 calculations (see Table S2 in the Supporting Information) confirm the conclusion that in
8 XT, DNXT and TNXT the oscillator strengths of the transitions from S_1 to higher excited
9 states do not noticeably differ. The simultaneous ultrafast decay of both S_2 and S_3 states in
10 DNXT would lead to vanishing of ESA band in the transient absorption spectra (see Figure
11 5). Thus, only the transitions from one state of the doublet can proceed in ultrafast mode.
12 Since the ultrafast decrease of ESA is much smaller than the decrease of SE, we need to
13 assume that there are at least two ultrafast channels $S_3 \rightarrow S_2$ and $S_3 \rightarrow Ds_1$. Adding these
14 two transitions together with the internal conversion channel $S_2 \rightarrow S_0$ to the simplest scheme
15 gives a new kinetic scheme which is used in the fit to the transition spectra in DNXT.
16
17
18
19
20
21
22
23
24
25
26
27
28

29 The kinetic scheme presented in Figure 4 describes the population state dynamics and it
30 can be written in the differential form:
31
32
33

$$34 \quad \frac{dS_3(t)}{dt} = -\frac{S_3(t)}{\tau_{IC32}} - \frac{S_3(t)}{\tau_{IC3D}} \quad (7)$$

$$38 \quad \frac{dS_2(t)}{dt} = -\frac{S_2(t)}{\tau_{IC21}} - \frac{S_2(t)}{\tau_{IC2D}} - \frac{S_2(t)}{\tau_{IC20}} + \frac{S_3(t)}{\tau_{IC32}} \quad (8)$$

$$41 \quad \frac{dS_1(t)}{dt} = -\frac{S_1(t)}{\tau_{ISC1}} + \frac{S_2(t)}{\tau_{IC21}} \quad (9)$$

$$45 \quad \frac{dT_1(t)}{dt} = \frac{S_1(t)}{\tau_{ISC1}} \quad (10)$$

$$48 \quad \frac{dDs_1(t)}{dt} = \frac{S_2(t)}{\tau_{IC2D}} + \frac{S_3(t)}{\tau_{IC3D}} \quad (11)$$

51 where $S_i(t)$, $T_1(t)$, and $Ds_1(t)$ stand here for the populations of corresponding states, τ_{IC32} ,
52 τ_{IC21} , τ_{IC3D} , τ_{IC2D} , τ_{IC20} and τ_{ISC1} are the time constants of the internal conversion and
53 intersystem crossing, respectively. The initial population of all states are zero except for
54
55
56
57
58
59
60

$S_3(0) = 0.4$ and $S_2(0) = 0.6$. The latter are determined by the oscillator strengths of the optical transitions and the frequency of the excited pulse since the splitting of the states S_3 and S_2 is pretty small and both states can be populated by single pulse.

The set of the parameters utilized in the calculations corresponds to the experimental setup: $k_B T = 0.25$ eV, $\Omega_{\text{hf}} = 0.15$ eV, $\omega_e = 3.1$ eV, $\tau_e = \tau_p = 100$ fs, $V_e = 0.005$ eV, $V_p = 0.015$ eV. The vibrational frequencies have been obtained from the DNXT fluorescence band structure. The relaxation time constants and weights of the solvent modes conform to acetonitrile: $\tau_1 = 100$ fs, $\tau_2 = 600$ fs, $x_1 = 0.6$, $x_2 = 0.4$.

Table 5: The model parameters returned from fitting TA spectra of DNXT in acetonitrile (see eq 2). f_i , E_{ri} , E_{rhi} , ΔG_i , and E_{max} are the weight, the reorganization energy of the medium, the reorganization energy of intramolecular high frequency vibrational modes, free energy change, and the energy of the maximum of the corresponding band after relaxation, respectively. All the energies are given in eV.

No	i	f_i	transition	$P(t)$	E_{ri}	E_{rhi}	ΔG_i	E_{max}
1	TTA	1.3	$T_1 \rightarrow T_k$	$T_1(t)$	0.12	0.09	-2.36	2.57
2	DSA	0.85	$DS_1 \rightarrow S_j$	$DS_1(t)$	0.14	0.09	-2.28	2.51
3	ESA2	0.9	$S_1 \rightarrow S_j$	$S_1(t)$	0.12	0.05	-1.86	2.03
4	ESA1	0.85	$S_{2,3} \rightarrow S_j$	$S_3(t) + S_2(t)$	0.11	0.05	-1.85	2.01
5	SE	0.73	$S_0 \leftarrow S_2$	$S_3(t) + S_2(t)$	0.10	0.40	-2.88	2.38
6	BL	0.4	$S_2 \rightarrow S_0$	$1.0 - DS_1$	0.10	0.40	-2.88	3.38

Analysis of the simulation results pictured in Figure 5 shows that the negative TA signal in the area around 500 nm predominantly consists of the stimulated emission $S_2 \rightarrow S_0$. An overlapping of the dark state absorption with stimulated emission bands is considerable at all time delays from 0.4 to 100 ps. The triplet – triplet absorption rises and leads to a positive signal in this region at the time delays from 10 to 100 ps. The TA dynamics is governed by several processes: the internal conversion between singlet states, the singlet – triplet intersystem crossing, and the transitions from the local singlet excited states (S_2 and S_3) to the singlet dark state. Figure 4 shows the minimal scheme including these processes along with the time constants returned from the fitting. The dark state absorption

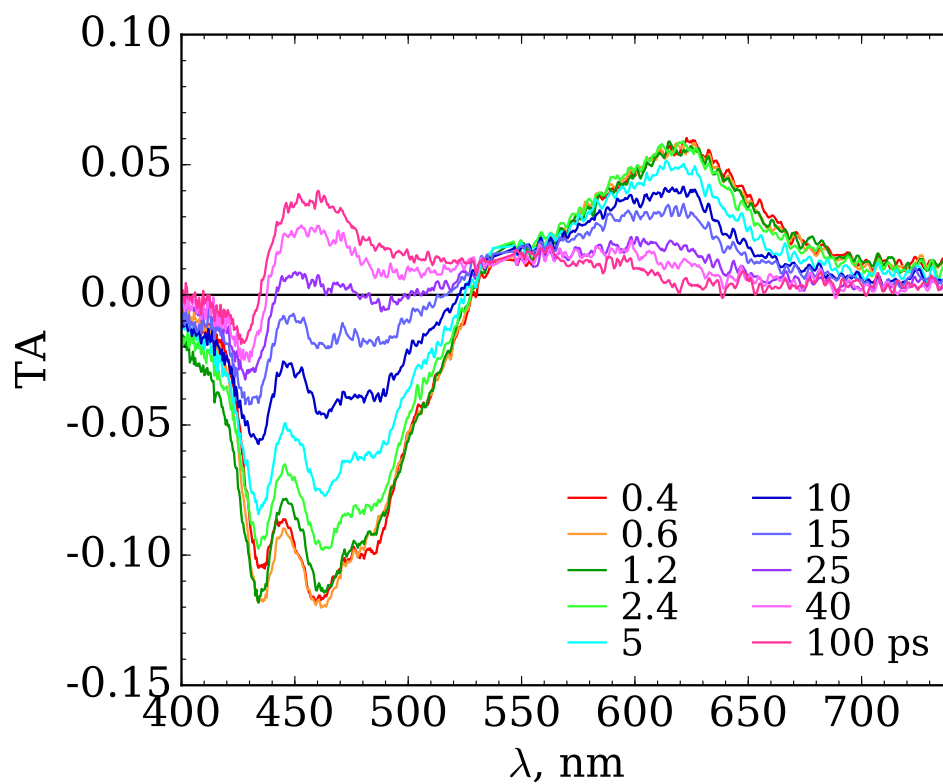


Figure 6: The experimental transient absorption spectra of XT in acetonitrile measured at 293 K.

1
2
3 band overlapping the stimulated emission at early time delays plays important role in the
4 suppression of stimulated emission at 0.4 ps. Due to the different initial population of S_3 and
5 S_2 states and fast transitions between the S_3 state and both S_2 and Ds_1 states the fitting at
6 early time delays reproduces the experimental signal. The measurements performed at other
7 TA experiment including wavelength region from 300 to 550 nm reveal the bleach dynamics.
8 It is seen the bleach signal is unchanged at the time delays from 1 to 100 ps. So the dark
9 state does not decay at the time under consideration (100 ps) and decreasing of the negative
10 TA signal can be caused by increasing dark state absorption.

11
12
13 The positive TA signal in the wavelength region from 580 to 700 nm is the excited state
14 absorption band including the absorption both the S_3 and S_2 states. The positive signal
15 at the red wing can be explained to the S_3 and S_2 absorption with the low energies of
16 transitions. The decreasing of the positive signal reflects the depopulation of the S_2 state
17 with $\tau_{IC21} = 17$ ps time constant to be close to the same time constant in the XT. The minor
18 shift of the band maximum from 632 nm to 625 nm is caused by increasing of the S_1 state
19 absorption. The irreversible intersystem crossing between the S_1 and T_i states results in
20 decreasing the positive signal up to zero after the time delay exceeding 40 ps. The fitting
21 gives the intersystem transition time constant $\tau_{ISC1} = 26$ ps. But the nearly white noise in
22 the region from 550 to 750 nm can distort the estimation of these time constants.

23
24
25 The kinetic scheme of the transitions is shown in Figure 4. It includes the dark state
26 and describes a lot of aspects of the TA dynamics in both the time and energetic domains.
27 The change in the initial population of the states S_3 and S_2 at the pumping stage allows
28 controlling the dynamics of the population of both the dark and triplet states. The excluding
29 of the dark state gives the kinetic scheme used to reproduce the TA signal of XT in n-hexane
30 where the intersystem time constant is smaller then presented here.

31
32
33 To demonstrate the effect of nitro-group on the excited state dynamics, let us compare
34 the spectral dynamics of DNXT and XT shown in Figures 5 and 6. The spectra in Figure 6
35 are close to that reported in ref 3. The XT transient spectra consist of three main parts:
36
37
38

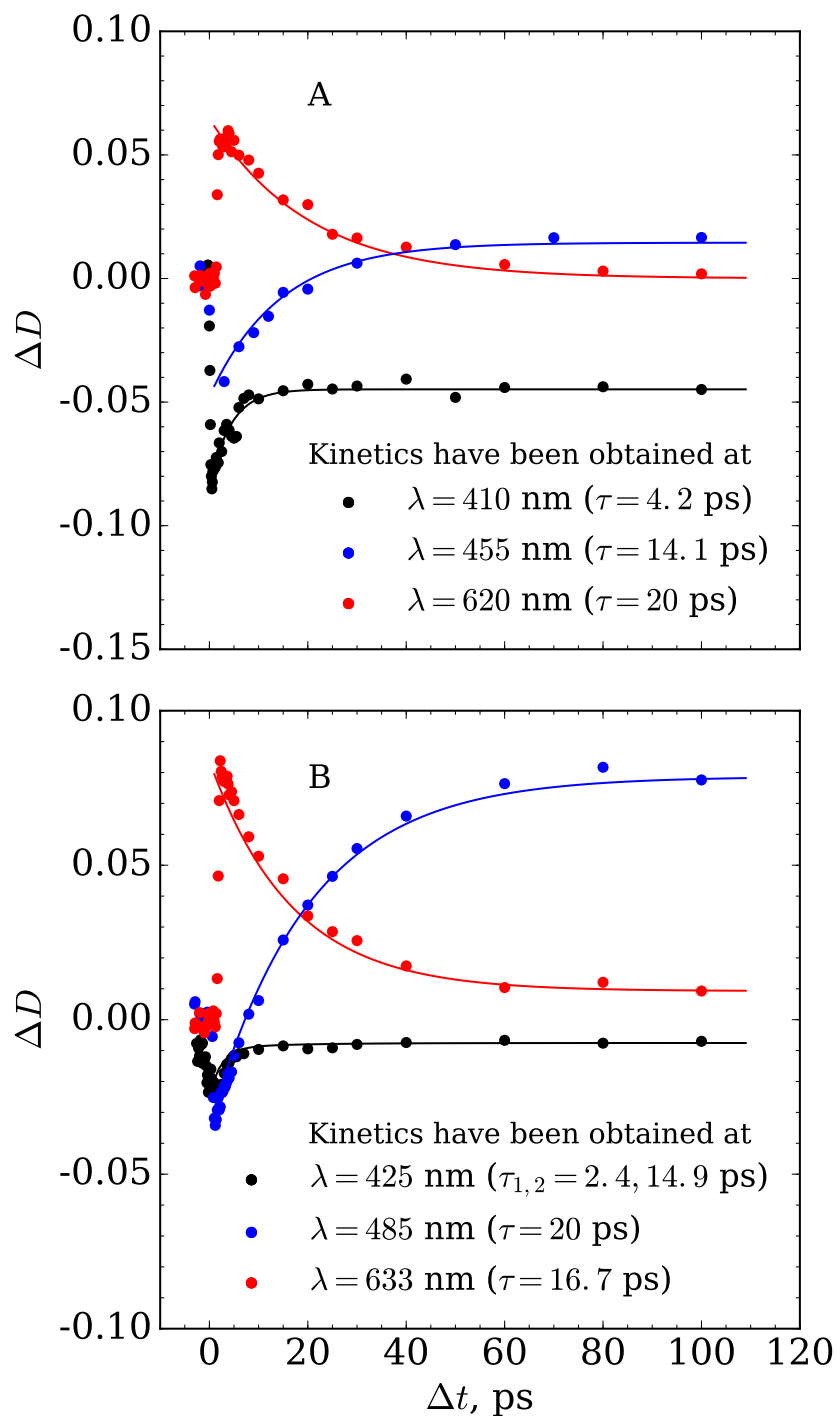


Figure 7: The kinetics of XT (Frame A) and DNXT (Frame B) measured experimentally (points) and their best fit (lines) in acetonitrile.

1
2
3 the negative band with a decay time about 14 ps (in the range 410 – 510 nm), the positive
4 absorption band with a decay time about 20 ps (in the range 540 – 740 nm), and the
5 positive long-lived triplet-triplet absorption band (in the range 410 – 520 nm). The decay
6 of the band in the range 410 – 510 nm well agrees with the time constant of the internal
7 conversion $S_2 \rightarrow S_1$, $\tau_{IC21} = 14$ ps, obtained from the fit within the simplest scheme. The
8 time constant of intersystem crossing $S_1 \rightarrow T_1$ is $\tau_{ISC1} = 18$ ps, so there is a considerable
9 population of S_1 state within the time interval 10 – 40 ps. Since the peaks of the ESA bands
10 from S_2 and S_1 are close each other, the decay of the band in the range 540 – 740 nm is
11 slower than the decay of SE.
12
13
14
15
16
17
18
19
20

21 The addition of the third nitro-group to the DNXT molecule leads to the C_{2v} symme-
22 try breaking, which results in significant changes in the TA spectra (see Figure S8 in SI).
23 First, the TA spectrum shifts to the red, so that the bleach signal becomes observable in
24 the experimental window. This agrees well with changes in stationary absorption spectra.
25 Second, the ESA spectra from the first and second singlet and triplet excited states are much
26 broader than the TA spectra in DNXT, apparently, because the symmetry breaking allows
27 for a series of new transitions. The general features of the spectral dynamics in TNXT are
28 similar to those observed in XT and DNXT. At the same time, the time constants of signal
29 decay at the characteristic wavelengths in TNXT are two or three times shorter than that
30 in XT and DNXT.
31
32
33
34
35
36
37
38
39
40

41 Figure 7 shows the kinetics of the transient absorption of XT and DNXT in acetonitrile
42 at the room temperature at a few characteristic wavelengths. One can see that the kinetics
43 at $\lambda = 425$ nm consists of two components with the time constants 2.4 and 14.9 ps in
44 DNXT (frame B in Figure 7), whereas in XT (Frame A) at $\lambda = 410$ nm it can be described
45 perfectly by single exponential function with time constant $\tau = 4.2$ ps. There is also the third
46 long-lived component caused by triplet-triplet absorption. This wavelength corresponds to
47 the long-wave edge of the steady-state $S_2 \leftarrow S_0$ absorption band. The complex dynamics
48 at 425 nm results from the overlapping of the bleach with triplet-triplet absorption bands,
49
50
51
52
53
54
55
56
57
58
59
60

1
2
3 depopulation of S_2 state, and solvent relaxation. This is the reason of the difference between
4 the time constants obtained from fitting of signal dynamics at a specific wavelength and the
5 time constants returned from fitting of spectral dynamics in the total spectral range. The
6 approach adopted here is based on fitting the spectral dynamics in the entire window of the
7 wavelengths, which returns from the fitting the true time constants of decay and population
8 of electronic states involved in the photochemical process. Just these time constants are in
9 use in chemical kinetics, while the time constants obtained from fitting the signal dynamics
10 at a certain wavelength are indirectly related to the kinetic characteristics of the electronic
11 transition.
12
13
14
15
16
17
18
19
20
21
22

23 Conclusions

24
25
26 The current research has uncovered ultrafast fluorescence quenching of the second excited
27 state in DNXT occurring on shorter timescale than that of the time resolution of the setup
28 exploited. This follows from a comparison of the stimulated emission signals of DNXT and
29 XT at early times. The stimulated emission signal of DNXT is about 3.5 times less than
30 that in XT at the delay of 0.4 ps. Since the fluorescence oscillator strength of the stimulated
31 emission in DNXT is only 1.8 times less than that in XT, the difference can not be explained
32 by a decrease of the oscillator strength. The discrepancy is rationalized in terms of ultrafast
33 depopulation of a new state, S_3 , located slightly higher than the second excited state. The
34 decay of this state results in ultrafast population of both the lower component of the doublet,
35 S_2 , and the dark state, Ds_1 , with comparable rates. The decay of the lower component of
36 the doublet S_2 leads to a slower decay of the stimulated emission with a time constant close
37 to that of the decay of ESA which is about 20 ps.
38
39
40
41
42
43
44
45
46
47
48
49

50 On the base of the doublet structure of the second excited state including the S_2 and
51 S_3 states along with a dark state, revealed by quantum chemical calculations, as well as S_1 ,
52 and T_1 states, a scheme of energy levels and transitions between them has been constructed,
53
54
55
56
57
58
59
60

1
2
3 which is used to fit the TA spectra. Due to the fact that the doublet, S_2 and S_3 , of DNXT
4 is populated by excitation pulse that is followed by a rapid transfer of population from S_3
5 to S_2 and the dark state, it is possible to achieve a slow decrease of the intense ESA band
6 in the vicinity of 630 nm. In the scheme, the higher level of the doublet is non-radiatively
7 coupled with S_2 and the dark state, while S_2 is connected with S_1 and Ds_1 states. The
8 ultrafast decay channel, $S_3 \rightarrow Ds_1$, and slower channels, $S_2 \rightarrow S_1$ and $S_2 \rightarrow Ds_1$, explain the
9 two stage nature of the fluorescence decay. At the same time, the transition $S_2 \rightarrow S_1$ occurs
10 at a rate close to that in XT. In the scheme, the dark state decay is neglected, since Ds_1 ,
11 in contrast to S_2 and T_1 states, is characterized by a considerable charge transfer from XT
12 scaffold to nitro-groups that can be the reason why the dark state is weakly coupled to S_2
13 and T_1 states.
14
15
16
17
18
19
20
21
22
23
24

25 The doublet structure of the second excited state has been predicted by quantum-chemical
26 calculations not only for DNXT but also for 2,7-diaminoxanthone.¹⁹ Here a fairly complex
27 scheme of electronic transitions in excited DNXT has been suggested. The scheme involves
28 two relatively long-lived excited states, the dark singlet and lower triplet states. The popu-
29 lations of these states can be controlled by changing the carrier frequency of the pump pulse,
30 since the change leads to a change in the initial populations of the S_3 and S_2 states, which,
31 in turn, leads to a change in Ds_1 and T_1 populations. Supposing the scheme is true, XT
32 derivatives like DNXT can be promising molecules for design of optical molecular switches.
33 For further verification of the proposed electronic transition scheme, additional experimental
34 studies are needed, for example, the study of the effect of variation of carrier frequency of
35 the exciting pulse within the absorption band on the spectral dynamics. Such a variation
36 should change the populations of the states of the doublet, which will lead to significant
37 changes in the kinetics of transitions and TA dynamics.
38
39
40
41
42
43
44
45
46
47
48
49
50
51
52
53
54
55
56
57
58
59
60

Supporting Information

Transient absorption spectra of DNXT in various solvents (polar and apolar), the results of measurements and calculations of TNXT stationary absorption and fluorescence (n-hexane) and transient absorption (acetonitrile) spectra, the structure of HOMO and LUMO of TNXT, the details of "lambda diagnostic", the diagram of TNXT energy levels calculated in the gas phase and the time-dependent signal kinetics of TNXT in acetonitrile obtained at certain wavelengths, a comparison of the calculated oscillator strengths of the transitions for three considered compounds (XT, DNXT and TNXT) with their energies of electronic transitions.

Acknowledgement

The study was performed by a grant from the Russian Science Foundation (Grant No. 16-13-10122). This work was partially supported by the Belarusian Republican Foundation for Fundamental Research (Grant No. P18R-202).

References

- (1) Milewski, M.; Sikorski, M.; Maciejewski, A.; Mir, M.; Wilkinson, F. Primary Photo-physical Properties of 4H-1-benzopyran- 4-thione in Cyclodextrin Complexes. *J. Chem. Soc., Faraday Trans.* **1997**, *93*, 3029–3034.
- (2) Szymanski, M.; Balicki, M.; Binkowski, M.; Kubicki, J.; Maciejewski, A.; Pawlowska, E.; Wrozowa, T. Effects of Solute-Solvent Interactions on Radiationless Decay of Thioketones Excited to Their S_2 - and T_1 -states. *Acta Phys. Pol. A* **1996**, *89*, 527–546.
- (3) Lorenc, M.; Maciejewski, A.; Ziolk, M.; Naskrecki, R.; Karolczak, J.; Kubicki, J.; Ciesielska, B. Mechanism and Deactivation Kinetics of S_2 -xanthione in Acetonitrile, a Quenching Solvent, and of S_2 -exciplex Measured by Pico- and Femtosecond Laser Spectroscopy. *Chem. Phys. Lett.* **2001**, *346*, 224–232.
- (4) Burdzinski, G.; Maciejewski, A.; Buntinx, G.; Poizat, O.; Lefumeux, C. Nature of the S_2 -state Quenching Process of Benzopyranthione by Hydrocarbon Solvents Measured by Pico- and Femtosecond Laser Spectroscopy. *Chem. Phys. Lett.* **2003**, *368*, 745–753.
- (5) Vieira Ferreira, L.; Ferreira Machado, I.; Oliveira, A.; Silva, J. D.; Krawczyk, A.; Sikorski, M. Surface Photochemistry: Diffuse Reflectance Studies of Thioketones Included into p-tert-butylcalix[6 and 8]arenes. *J. Mol. Struct.* **2007**, *827*, 11–19.
- (6) Fedunov, R. G.; Rogozina, M. V.; Khokhlova, S. S.; Ivanov, A. I.; Tikhomirov, S. A.; Bondarev, S. L.; Raichenok, T. F.; Buganov, O. V.; Olkhovik, V. K.; Vasilevskii, D. A. Electronic Structures and Population Dynamics of Excited States of Xanthione and Its Derivatives. *Chem. Phys.* **2017**, *494*, 1–10.
- (7) Maciejewski, A.; Steer, R. P. The Photophysics, Physical Photochemistry, and Related Spectroscopy of Thiocarbonyls. *Chem. Rev.* **1993**, *93*, 67–98.

- 1
2
3
4 (8) Maciejewski, A.; Milewski, M.; M.Szymanski, A Method of Determination of Quantum
5 Yields of $S_3 \rightarrow S_2$, $S_3 \rightarrow S_1$, and $S_3 \rightarrow S_0$ Intramolecular Radiationless Transitions. *J.*
6 *Chem. Phys.* **1999**, *111*, 8462–8468.
7
8
9
10 (9) Kasha, M. Characterisation of Electronic Transitions in Complex Molecules. *Discuss.*
11 *Faraday Soc.* **1950**, *9*, 14–19.
12
13
14
15 (10) Eisenberger, H.; Nickel, B.; Ruth, A. A.; Steer, R. P. Photophysical Triplet State
16 Processes of 4-H-1-benzopyrane-4-thione in a Perfluoroalkane. Part 2. – Delayed $S_2 \rightarrow$
17 S_0 Fluorescence Due to Triplet-Triplet Annihilation. *J. Chem. Soc., Faraday Trans. 2*
18 **1996**, *92*, 741–746.
19
20
21
22
23 (11) Kumar, C. V.; Qin, L.; Das, P. K. Aromatic Thioketone Triplets and Their Quenching
24 Behaviour Towards Oxygen and Di-*t*-butylnitroxyl Radical. A Laser-Flash-Photolysis
25 Study. *J. Chem. Soc., Faraday Trans. 2* **1984**, *80*, 783–793.
26
27
28
29
30 (12) Vavilov, S. I. Die Fluoreszenzausbeute von Farbstofflösungen. *Z. Phys.* **1924**, *22*, 266.
31
32
33 (13) Nickel, B.; Eisenberger, H.; Wick, M.; Steer, R. Photophysical Triplet State Processes
34 of 4H-1-benzopyrane-4-thione in a Perfluoroalkane. Part 3. – Excitation-Wavelength
35 Dependence of Luminescence Quantum Yields. *J. Chem. Soc., Faraday Trans.* **1996**,
36 *92*, 1101–1104.
37
38
39
40
41 (14) Plotnikov, V. The Nucleobases of DNA System with an Abnormally Fast Process of
42 Internal $S_1 \rightarrow S_0$ -Conversion. *DAS USSR* **1990**, *310*, 1403–1407, (in Russian).
43
44
45
46 (15) Martynov, I.; Demyashkevich, A.; Uzhinov, B.; Kuzmin, M. Reactions of Proton Trans-
47 fer in Excited Electronic States. *Advances in Chemistry* **1977**, *46*, 3–31, (in Russian).
48
49
50
51 (16) Rai-Constapel, V.; Etinski, M.; Marian, C. Photophysics of Xanthone: A Quantum
52 Chemical Perusal. *J. Phys. Chem. A* **2013**, *117*, 3935–3944.
53
54
55
56
57
58
59
60

- 1
2
3 (17) Cavaleri, J.; Prater, K.; Bowman, R. An Investigation of the Solvent Dependence on
4 the Ultrafast Intersystem Crossing Kinetics of Xanthone. *Chem. Phys. Lett.* **495–502**,
5 *259*, 1996.
6
7
8
9
10 (18) Mundt, R.; Villnow, T.; Ziegenbein, C.; Gilch, P.; Marian, C.; Constapel, V. Thiox-
11 anthone in Apolar Solvents: Ultrafast Internal Conversion Precedes Fast Intersystem
12 Crossing. *Phys. Chem. Chem. Phys.* **2016**, *18*, 6637–6647.
13
14
15
16 (19) Bondarev, S. L.; Tikhomirov, S. A.; Raichenok, T. F.; Bugarov, O. V.; Fedunov, R. G.;
17 Khokhlova, S. S.; Ivanov, A. I.; Ol'khovik, V. K.; Galinovskii, N. A. Fluorescence
18 Quenching of 2,7-diaminoxanthone in Alcohols by Hydrogen Bonding: An Experimental
19 and Theoretical Research. *J. Lumin.* **2018**, *198*, 226–235.
20
21
22
23
24 (20) Wallin, S.; Monnereau, C.; Blart, E.; Gankou, J.-R.; Odobel, F.; Hammarström, L.
25 State-Selective Electron Transfer in an Unsymmetric Acceptor-Zn(II)porphyrin-
26 Acceptor Triad: Toward a Controlled Directionality of Electron Transfer from Por-
27 phyrin S_2 and S_1 States as a Basis from Molecular Switch. *J. Phys. Chem. A* **2010**,
28 *114*, 1709–1721.
29
30
31
32 (21) Muller, P.-A.; Vauthey, E. Charge Recombination Dynamics of Geminate Ion Pairs
33 Formed by Electron Transfer Quenching of Molecules in an Upper Excited State. *J.*
34 *Phys. Chem. A* **2001**, *105*, 5994–6000.
35
36
37 (22) Feskov, S. V.; Mikhailova, V. A.; Ivanov, A. I. Non-Equilibrium Effects in Ultrafast
38 Photoinduced Charge Transfer Kinetics. *J. Photochem. Photobiol. C* **2016**, *29*, 48–72.
39
40
41
42 (23) Scheibye, S.; and S.-O. Lawesson, R. S.; Rømming, C. Studies on Organophospho-
43 rus Compounds – XL: Reactions of Ketones with 2,4-bis(4-methoxyphenyl)-1,3,2,4-
44 dithiadiphosphetane 2,4-disulfide. *Tetrahedron* **1982**, *38*, 993–1001.
45
46
47
48 (24) Borisevich, E.; Knyukshto, V.; Kozyrev, A.; Solovev, K. The Influence of External
49
50
51
52
53
54
55
56
57
58
59
60

- 1
2
3 Bromine Atoms on Photophysical Processes and NH-Shift in Porphyrine Macrocycle.
4
5 *Opt. Spectr.* **1993**, *74*, 129–135.
6
7
- 8 (25) Borisevich, N.; Bouganov, O.; Tikhomirov, S.; Tolstorozhev, G.; Shkred, G. Passive
9
10 Mode Locking of a Femtosecond Ti:Sapphire Laser with Pulsed Synchronous Pumping
11
12 by a Finite Train of Picosecond Pulses. *Quantum Electronics* **1999**, *29*, 780–786, (in
13
14 Russian).
15
- 16 (26) Stsiapura, V.; Kurhuzenkau, S.; Kuzmitsky, V.; Bouganov, O.; Tikhomirov, S. Solvent
17
18 Polarity Effect on Nonradiative Decay Rate of Thioflavin T. *J. Phys. Chem. A* **2016**,
19
20 *120*, 5481–5496.
21
22
- 23 (27) Schmidt, M. W.; Baldrige, K. K.; Boatz, J. A.; Elbert, S. T.; Gordon, M. S.;
24
25 Jensen, J. H.; Koseki, S.; Matsunaga, N.; Nguyen, K. A.; Su, S. et al. General Atomic
26
27 and Molecular Electronic Structure System. *J. Comput. Chem.* **1993**, *14*, 1347–1363.
28
29
- 30 (28) Gordon, M. S.; Schmidt, M. W. In *Theory and Applications of Computational Chem-*
31
32 *istry: The First Forty Years*; Dykstra, C. E., Frenking, G., Kim, K. S., Scuseria, G. E.,
33
34 Eds.; Elsevier: Amsterdam, 2005; pp 1167–1189.
35
36
- 37 (29) Peach, M. J. G.; Benfield, P.; Helgaker, T.; Tozer, D. J. Excitation Energies in Density
38
39 Functional Theory: An Evaluation and a Diagnostic Test. *J. Chem. Phys.* **2008**, *128*,
40
41 044118.
42
43
- 44 (30) Bellamy, L. J. In *The Infra-Red Spectra of Complex Molecules*, 3rd ed.; Krimm, S., Ed.;
45
46 Wiley: New York, 1976; p 433.
47
48
- 49 (31) Fedunov, R. G.; Ivanov, A. I. Influence of Spectral Characteristics of the Pump Pulse
50
51 on the Transient Absorption of Donor-Acceptor Complexes in Polar Solvents. *J. Russ.*
52
53 *Laser Res.* **2012**, *33*, 152–165.
54
55
56
57
58
59
60

- 1
2
3 (32) Fedunov, R. G.; Plotnikova, A.; Ivanov, A. I.; Vauthey, E. Simulations of the Ultrafast
4 Transient Absorption Dynamics of a Donor-Acceptor Biaryl in Solution. *J. Phys. Chem.*
5 *A* **2017**, *121*, 471–481.
6
7
8
9
10 (33) Horng, M. L.; Gardecki, J. A.; Papazyan, A.; Maroncelli, M. Subpicosecond Measure-
11 ments of Polar Solvation Dynamics: Coumarin 153 Revisited. *J. Phys. Chem.* **1995**,
12 *99*, 17311–17337.
13
14
15
16
17
18
19
20
21
22
23
24
25
26
27
28
29
30
31
32
33
34
35
36
37
38
39
40
41
42
43
44
45
46
47
48
49
50
51
52
53
54
55
56
57
58
59
60

Graphical TOC Entry

